J Therm Anal Calorim
DOI 10.1007/s10973-015-4749-z

The preparation and characterization of dichlorobispyridinecopper(II) complex and its intermediates

Thermal and kinetic investigations by non-isothermal methods

T. Yesilkaynak[1] · F. M. Emen[2] · G. Avsar[3] · N. Kulcu[3]

Received: 3 February 2015 / Accepted: 3 May 2015

Abstract The dichlorobispyridinecopper(II) complex, $[CuPy_2Cl_2]$, and its decomposition intermediates were synthesized and characterized by MALDI-TOF MS, far-IR, reflectance UV, atomic absorption spectroscopy techniques. The thermal decomposition reactions of the $[CuPy_2Cl_2]$ were investigated by differential thermal analysis (DTA)/thermogravimetry (TG) combined system. The intermediates and the final products were analyzed by high-temperature X-ray powder diffraction (HT-XRD) technique. The XRD pattern of the complex indexed as $[CuPy_2Cl_2]$ (PDF: 00-014-991) has a monoclinic crystal system, P21/n (14) space group with $a = 16.9673$ Å, $b = 8.5596$ Å, $c = 3.8479$ Å; $\alpha = \gamma = 90.00°$, $\beta = 91.98°$, $V = 558.51$ Å^3 and $Z = 2.00$. After comparison of thermogravimetric results of the $[CuPy_2Cl_2]$, the decomposition mechanism was suggested. The intermediates were prepared separately at 217 and 245 °C temperatures which were chosen from TG curve by using a tube furnace under N_2 atmosphere and characterized. The spectroscopic results reveal that the structure of the intermediates to be $[CuPyCl_2]$ and $[CuPy_{2/3}Cl_2]$ formulas (hereafter abbreviated as 2 and 3, respectively). MALDI-TOF MS spectra of the 2 and 3 show $[M+H]^+$ ($m/z = 214.978$) and $[M-H]^+$ ($m/z = 185.614$), $[M+C_2H_3O]^+$ ($m/z = 221.002$) molecular ion peaks which correspond to suggested structure for 2 and 3, respectively. Also, HT-XRD results revealed that the 2 and 3 are new phases and there is no any certain information of these phases in the literature. The values of the activation energy, E_a, were calculated by model-free (Kissenger–Akahira–Sunose, Flyn–Wall–Ozawa) methods for all decomposition stages.

Keywords Complexes · Pyridine complexes · Thermal analysis · Transition metal–halides

Introduction

3-d transition metal complexes have been a subject of study of many researchers for a long time. One of the subjects to scrutiny is mixed complexes of pyridine derivatives. The studies of the complexes with pyridine derivatives and divalent transition metal ions such as Cr, Mn, Co, Ni and Cu have been started in the 1960s. The initial works focused on their synthesis and characterization using UV–Vis, IR and NMR techniques. Transition metal–halogen complexes of pyridine derivative ligands such as pyridine, 2-chloropyridine, 2-bromopyridine, 3-chloropyridine, 3-bromopyridine, 2-methoxypyridine [1], 2-(p-tolyl)pyridine [2], 2-methylpyridine, 3-methylpyridine, 3,4-dimethylpyridine [3], 4-benzoylpyridine,3-hydroxypyridine, 4-ethylpyridine [4] were synthesized and characterized in previous studies. One of them has focused on the identification of intermediate products of cobalt(II) pyridine derivative complexes, and mechanism of decomposition reactions has been proposed as follows [5]:

✉ T. Yesilkaynak
tyesilkaynak@ksu.edu.tr

[1] Afsin Vocational High School, Sutcu Imam University, 46500 Kahramanmaras, Turkey

[2] Department of Chemistry, Faculty of Arts and Science, Mehmet Akif Ersoy University, 15030 Burdur, Turkey

[3] Department of Chemistry, Faculty of Arts and Science, Mersin University, 33343 Mersin, Turkey

Published online: 25 June 2015

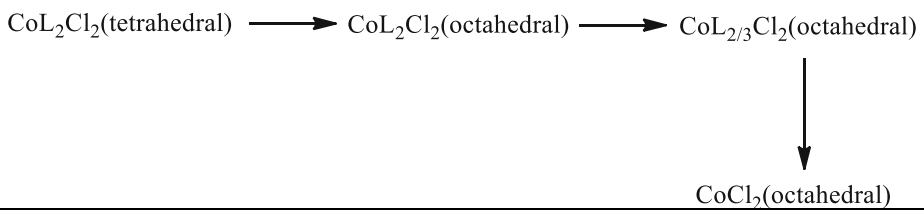

Furthermore, it is claimed that the intermediate $CoL_{2/3}Cl_2$ has polymeric structure involving Co–Cl–Co bridges [5–16]. The chlorocuprate complexes that contain copper atoms with a single coordination geometry, both in polymeric and in monomeric compounds, have so far been reported by researchers [6–10]. Some copper complexes such as $(HPy)_2[Cu_3Cl_8(H_2O)_2]$, $[CuPyCl_2]$ and $[CuPy_2Cl_2]$ were prepared by chemical methods and investigated by spectroscopic and thermal analysis techniques [11].

The thermal stability and the thermal decomposition reactions of pyridine derivative complexes were studied by thermal analysis methods [4, 12–15, 18, 19]. In these reactions, the starting compounds have been well known for a long time, but the structure of the intermediate products of the degradation has not been fully explained and also the kinetics of the decomposition reactions have not been explored [12–22].

In the present study, dichlorobispyridinecopper(II) complex, $[CuPy_2Cl_2]$, and its intermediates (2 and 3) formed during thermal decomposition of the $[CuPy_2Cl_2]$ were prepared and characterized by MALDI-TOF MS, far-IR, diffuse reflectance UV, elemental analysis, atomic absorption spectrometer (AAS) and HT-XRD techniques. The DTA/TG system was used for the investigation of the thermal decomposition reactions. Further, the kinetic parameters of the decompositions were determined by KAS and FWO methods.

Experimental

Synthesis of the $CuPy_2Cl_2$

Dichlorobispyridinecopper(II) complex, $[CuPy_2Cl_2]$, was prepared according to the literature [2, 3, 14]. The reaction equation is given as below:

$$CuCl_2 + 2Py \xrightarrow[[Ethanol]]{70^{\circ}C} [CuPy_2Cl_2] \quad (1)$$

A solution of copper(II) chloride (0.025 mol) in ethanol (40 cm^3) was added dropwise to solution of pyridine (0.05 mol) in ethanol (20 cm^3). The reaction mixture was heated under reflux for 2 h at constant temperature of 70 °C and then cooled to room temperature. The obtained complex was filtered and washed with ethanol and dried in a desiccator.

Synthesis of the intermediates (2 and 3)

The intermediates 2 and 3 were obtained at 217 and 245 °C determined from TG curves in a high-temperature furnace under N_2 atmosphere.

Dichlorobispyridinecopper(II), $[CuPy_2Cl_2]$ (Calc. for $C_{10}H_{10}N_2Cl_2Cu$: C, 41.04; N, 9.57; H, 3.44; Cu, 21.71. Found: C, 40.84; N, 9.57; H, 3.45; Cu, 21.28 %). Far-IR (KBr pellet, cm^{-1}): ν(Cu–Cl) 266, ν(Cu–N) 289, υ(Ar–C–H) 442 and 643.

The intermediate 2, $[CuPyCl_2]$ (Calc. for $C_5H_5NCl_2Cu$: C, 28.12; N, 6.56; H, 2.36; Cu, 29.76. Found: C, 26.68; N, 6.21; H, 2.31; Cu, 28.92 %). Far-IR (KBr pellet, cm^{-1}): ν(Cu–Cl) 259, ν(Cu–N) 288, υ(Ar–C–H) 441 and 638. Reflectance UV (nm): 250–350 (br.), 700 (br.). MALDI-TOF MS, *m/z*: $[M+H]^+$ (214.978).

The intermediate 3, $[CuPy_{2/3}Cl_2]$ (Calc. for $C_{10/3}H_{10/3}N_{2/3}Cl_2Cu$: C, 21.39; N, 4.99; H, 1.80; Cu, 33.95. Found: C, 20.80; N, 4.73; H, 1.84; Cu, 33.31 %). Far-IR (KBr pellet, cm^{-1}): ν(Cu–Cl) 252 and 332, ν(Cu–N) 287, υ(Ar–C–H) 439. Reflectance UV (nm): 250–300 (br.), 692 (br.). MALDI-TOF MS, *m/z*: $[M-H]^+$ (185.614), $[M+C_2H_3O]^+$ (221.002).

The intermediate 4, $(CuCl_2)$ Far-IR (KBr pellet, cm^{-1}): ν(Cu–Cl) 237, 286 and 334. Reflectance UV (nm): 359, 409, 446 (w).

Instrumentals

Microanalyses were obtained using a LECOCHNS-932 model instrument. MALDI-TOF MS spectra were recorded on Bruker Microflex LT MALDI-TOF MS instrument without using a matrix. Acetone was used as a solvent for intermediates. Far-IR spectra were recorded by Vertex 80 V instrument to investigate vibrations of Cu–N and Cu–Cl bonds. Diffuse reflectance UV spectrum was recorded by Varian Cary 100Bio to identify UV–Vis bands of the complex in solid state. GBC 933 AA AAS was used in the determination of amount of copper(II) ion in the complex and intermediates. Bruker D8 model high-temperature X-ray powder diffractometer ($CuK_{\alpha 1}$ light source) was used for the description of high-temperature phases of the

complex. The TG/DTA curves were recorded by a Shimadzu DTG-60H equipped with DTA and TG units. The thermal analysis system was used in the temperature range of from 25 to 1000 °C. The samples were placed in Pt crucibles, and α-Al_2O_3 was used as the reference material. Measurements were taken using a dynamic nitrogen furnace atmosphere at a flow rate of 50 mL min^{-1}. Different heating rates were chosen as 5, 10 and 15 °C min^{-1}, and the sample sizes vary in the mass range of 5–10 mg.

Results and discussion

Far-IR studies of the $[CuPy_2Cl_2]$

Far-IR measurement of the $[CuPy_2Cl_2]$ was taken in the range of 10–800 cm^{-1} to detect the presence of vibration for metal–halide and metal–nitrogen bond. Important far-IR peak data of the $[CuPy_2Cl_2]$ are given in experimental section. Far-IR spectrum of the $[CuPy_2Cl_2]$ shows two strong absorptions (266 and 289 cm^{-1}) ascribed to band stretching for ν(Cu–Cl) and ν(Cu–N) groups, respectively. The bending vibrations of υ(C–H) groups for pyridine rings also observed in 442 and 643 cm^{-1}.

Elemental analysis and atomic absorption studies of the $[CuPy_2Cl_2]$

Elemental analysis and atomic absorption spectroscopy methods were used for the characterization of complex composition. C, H, N and Cu amounts in the $[CuPy_2Cl_2]$ were determined (the results are given in experimental section). The calculated and experimental values for the $[CuPy_2Cl_2]$ are very close to each other, and as expected, the composition of the synthesized complex was formulated as $[CuPy_2Cl_2]$.

Thermal analysis (DTA/TG) of the $[CuPy_2Cl_2]$

Thermal decomposition reactions of the $[CuPy_2Cl_2]$ were investigated 10 °C min^{-1} heating rate and under N_2 atmosphere by DTA/TG instrument, and the DTA/TG curves and obtained results are shown in Fig. 1. The TG curve shows that the decomposition process of the $[CuPy_2Cl_2]$ takes place in four stages. The $[CuPy_2Cl_2]$ appears to be stable up to 130 °C determined from the TG curve. The first decomposition stage occurs in temperature range of 135–235 °C. In this step, the elimination of 1 mol pyridine ligand resulted in an experimental mass loss of 28.63 % (Calc.: 27.03 %). At the end of this stage, the intermediate 2 formed as given $[CuPyCl_2]$ formula. The second decomposition is observed in temperature range of 235–270 °C with mass loss of 9.01 % (Calc.: 8.64 %). At this stage, 1/3 mol pyridine ligand was broken up and turned into the gas products and formed intermediate 3 with $[CuPy_{2/3}Cl_2]$ formula. The third decomposition takes place between 270 and 350 °C with mass loss of 18.10 % (Calc.: 18.02 %) which corresponds to the elimination of 2/3 mol pyridine ligand. At the end of this stage, the intermediate 4 formulated as $CuCl_2$ was obtained. The last decomposition step is observed in temperature range of 350–650 °C. In this stage, the $CuCl_2$ may be converted to some polymeric metal–halide compounds (structurally unknown products). Thermoanalytical results of the decomposition reactions of the $[CuPy_2Cl_2]$ are given in Table 1. The DTA curve shows seven endothermic peaks. The minimum points of the endothermic peaks are 217, 245, 319, 380, 415 and 607 °C, respectively. The first four peaks belong to degradation of the complex, while the others correspond to decomposition and melting of the $CuCl_2$. It is well known that TG/DTA peaks of the chemical reactions move to higher temperatures as the heating rate increases. In the higher heating rate, the amount of gas diffusion around the sample material will be so low. Consequently, the local partial pressure of the sample will increase and the decomposition will take place at a higher temperature. This effect was investigated in the other thermal analysis studies in the literature [23–25]. The TG curves of the $[CuPy_2Cl_2]$ complex at different heating rates (5, 10, 15 °C min^{-1}) are shown in Fig. 2. The initial, final and peak temperature values of each decomposition stages of the $[CuPy_2Cl_2]$ are given in Table 2. Also, thermal decomposition reactions of the complex based on the TG data are recommended as follows:

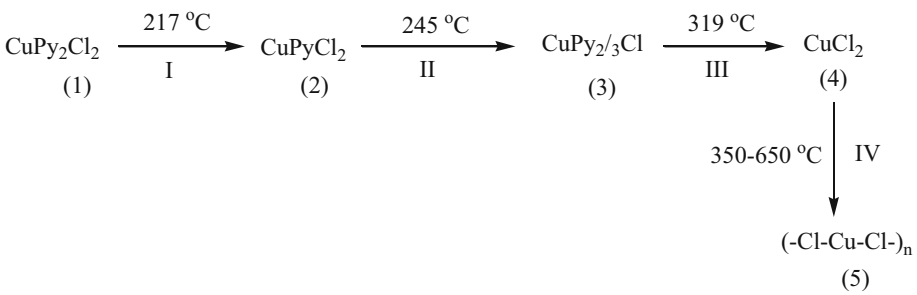

(2)

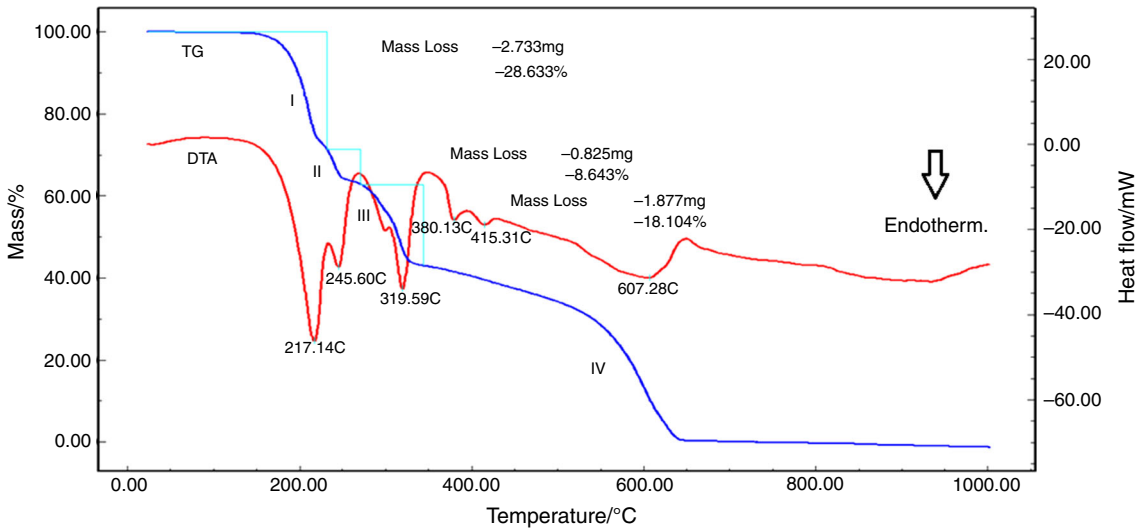

Fig. 1 DTA/TG curves and obtained results of the $CuPy_2Cl_2$

Table 1 Thermoanalytical results of the decomposition reactions of the $[CuPy_2Cl_2]$

Complex	Stage	DTA peak/°C	TG temp. range/°C	Mass loss/%		Evolved moiety
				Exper.	Theor.	
$[CuPy_2Cl_2]$	I	217	135–235	28.63	27.03	$-C_5H_5N$
	II	245	235–270	8.64	9.01	$-1/3C_5H_5N$
	III	319	270–350	18.10	18.02	$-2/3C_5H_5N$

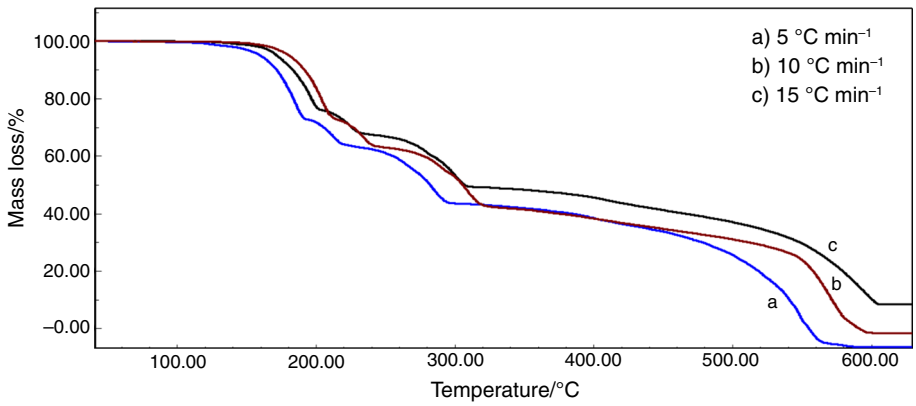

Fig. 2 The TG curves of the $[CuPy_2Cl_2]$ complex at different heating rates (5, 10, 15 °C min^{-1})

The synthesis temperatures of the intermediates (2 and 3) were chosen as 217 and 245 °C from DTA curve in order to clarify the structure of the intermediates. The complex was heated at these temperatures under nitrogen in a tube furnace, and intermediates (2 and 3) were prepared separately. The obtained intermediates were characterized by elemental analysis, AAS, far-IR, diffuse reflectance UV spectroscopy (these data are given in the experimental section), MALDI-TOF MS and HT-X-ray diffraction techniques. The results of elemental analysis and AAS measurements are in agreement with calculated values for the proposed structure of intermediates. Also, these results are consistent with the proposed thermal decomposition reactions.

Diffuse reflectance UV and MALDI-TOF MS studies of the intermediates (2, 3 and 4)

Diffuse reflectance UV spectroscopy measurements were taken in order to determine the coordination environment for intermediates 2, 3 and 4. The results are given in experimental section. The diffuse reflectance UV measurement of the intermediate 2 was taken from 200 to 800 nm.

Table 2 The initial, final and peak temperature values of each decomposition stages of the $[CuPy_2Cl_2]$

Decomposition stage	Peak temperature/°C	Heating rate, β/°C min^{-1}			Avg.
		5	10	15	
I	T_i	136	147	161	148
	T_f	193	212	226	201.33
	T_m	187	199	210	198.67
II	T_i	193	212	226	210.33
	T_f	223	246	257	242
	T_m	214	227	237	226
III	T_i	223	246	257	242
	T_f	298	323	337	319.33
	T_m	290	303	313	302

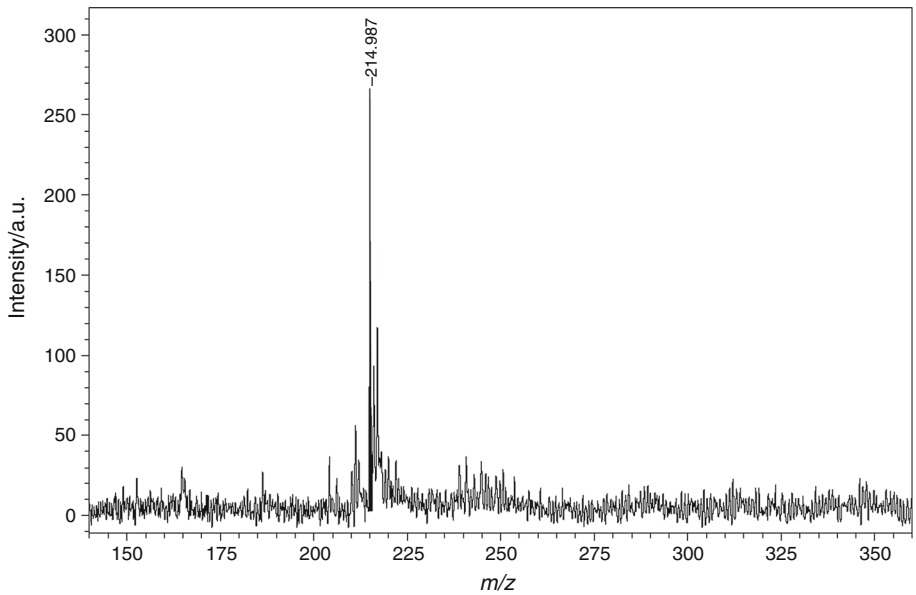

Fig. 3 MALDI-TOF MS spectrum of 2

The $N \rightarrow Cu^{2+}$ charge transfer transition observed between N of the pyridine ring and the central metal atom at 250–350 nm wavelength range [26]. The broad band is observed 700 nm (14,409 cm^{-1}) attributed to $^2A_{1g} \rightarrow {}^2B_{1g}$ and $^2B_{1g} \rightarrow {}^2E_g$ transitions which correspond to pseudo-tetrahedral coordination structure [27–29]. Diffuse reflectance UV spectrum of the intermediate 3 showed a broad band in the range of 250–300 nm. This band corresponds to charge transfer transitions of $N \rightarrow Cu^{2+}$. Another broad band is shown at 692 nm attributed to the pseudo-tetrahedral coordination structure like intermediate 2. Diffuse reflectance UV spectrum of the intermediate 4 shows three absorption bands at 359 nm (27,855 cm^{-1}), 409 nm (24,450 cm^{-1}) and 446 nm (24,421 cm^{-1}) which belong to square planar structure of the intermediate 4. These results show that four coordination numbers still were protected even if completely removing the pyridine ligands [30].

MALDI-TOF MS spectra were taken without using a matrix for 2 and 3 shown in Figs. 3 and 4. The molecular ion peaks were determined as $[M+H]^+$ ($m/z = 214.978$) for 2 and $[M-H]^+$ ($m/z = 185.614$) and $[M+C_2H_3O]^+$ ($m/z = 221.002$) for 3 (M represents 2 and 3 molecules). These results are in good agreement with proposed structure for 2 and 3.

Far-IR studies of the intermediates (2, 3 and 4)

Far-IR measurements were taken for the determination of the bond vibrations of metal–nitrogen (Cu–N) and metal–halogen (Cu–Cl) bonds of the intermediates (2 and 3). Important far-IR peak data are given in experimental

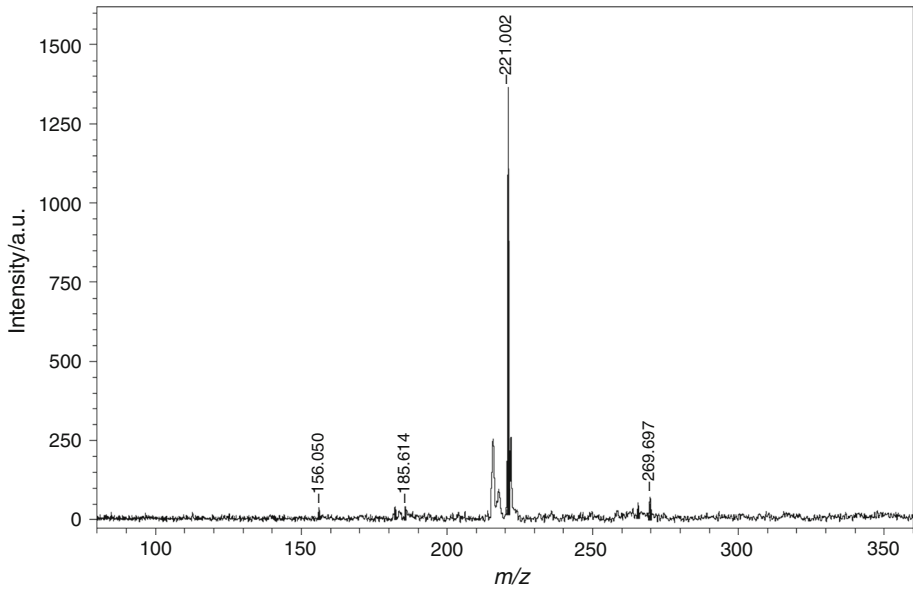

Fig. 4 MALDI-TOF MS spectrum of 3

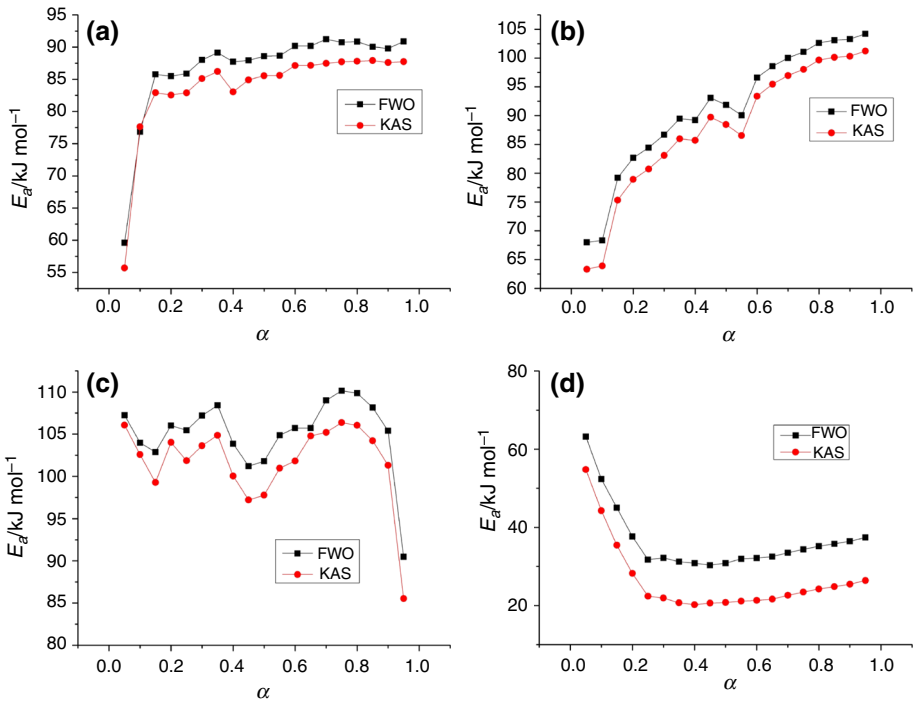

Fig. 5 The variation of the activation energy, E_a values with respect to decomposition ratio, α of the $CuPy_2Cl_2$ (**a** stage I, **b** stage II, **c** stage III and **d** stage IV)

section. In the far-IR spectrum of the complex, *ν*(Cu–Cl) and *ν*(Cu–N) stretching vibrations were observed at 289 and 266 cm^{-1}, while these values shifted to 288 and 259 cm^{-1} for intermediate 2, respectively. Also, *υ*(C–H) bending vibrations of the intermediate 2 shifted to 441 and 638 cm^{-1}. Unlike from the $[CuPy_2Cl_2]$, a new *ν*(Cu–Cl) vibration band was observed at 330 cm^{-1}. After one mole of pyridine removed, the intermediate 2 formed and new Cl–M–Cl bridges occurred. Further, the four coordination number still was reserved in this way [31]. In far-IR spectrum of the intermediate 3, the vibrations of *ν*(Cu–Cl), *ν*(Cu–N) and *υ*(C–H) were observed at 287, 252 and 439 cm^{-1}, respectively. However, unlike the intermediate 2, a new *ν*(Cu–Cl) band observed at 332 cm^{-1} for intermediate 3. This band was estimated to be Cl–M–Cl bond bridge like intermediate 2 [31]. Far-IR spectrum of the intermediate 4 ($CuCl_2$) showed that after complete separation of the pyridine ligands from the complex, *ν*(Cu–N) stretching bands were not observed. However, ν(Cu–Cl) vibrations were observed at 237, 286 and 334 cm^{-1}. These band vibrations correspond to the bridge bonding [31, 32].

Table 3 The activation energy, E_a, values at different decomposition stages of the $[CuPy_2Cl_2]$

α	FWO	R^2	KAS	R^2	FWO	R^2	KAS	R^2
Stage 1					*Stage 2*			
0.05	59.59	0.9893	55.69	0.9862	68.01	1.0000	63.33	1.0000
0.10	76.84	0.9161	77.63	0.9961	68.33	0.9999	63.92	0.9998
0.15	85.78	0.9842	82.91	0.9812	79.24	0.9992	75.33	0.9984
0.20	85.5	0.9702	82.55	0.9646	82.69	0.9974	78.93	0.9968
0.25	85.89	0.9644	82.9	0.9578	84.45	0.9963	80.75	0.9954
0.30	88.02	0.9613	85.1	0.9543	86.71	0.9938	83.1	0.9925
0.35	89.13	0.9720	86.22	0.9668	89.48	0.9957	85.99	0.9948
0.40	87.74	0.9741	83.05	0.9734	89.23	0.9940	85.71	0.9927
0.45	87.95	0.9793	84.91	0.9754	93.08	0.9928	89.73	0.9913
0.50	88.59	0.9826	85.56	0.9793	91.87	0.9951	88.45	0.9940
0.55	88.66	0.9825	85.61	0.9791	90.07	0.9955	86.55	0.9945
0.60	90.17	0.9861	87.16	0.9834	96.61	0.9908	93.39	0.9890
0.65	90.19	0.9907	87.17	0.9889	98.61	0.9894	95.48	0.9874
0.70	91.22	0.9920	87.49	0.9904	100.04	0.9873	96.97	0.9850
0.75	90.75	0.9928	87.72	0.9914	101.09	0.9888	98.06	0.9867
0.80	90.85	0.9991	87.81	0.9917	102.64	0.9901	99.68	0.9883
0.85	90.05	0.9908	87.93	0.989	103.11	0.9851	100.14	0.9824
0.90	89.78	0.9910	87.62	0.9892	103.3	0.9850	100.33	0.9828
0.95	90.87	0.9945	87.75	0.9934	104.22	0.9734	101.23	0.9688
Stage 3					*Stage 4*			
0.05	107.24	0.9567	106.07	0.9493	63.2	0.9626	54.77	0.9725
0.10	103.97	0.9795	102.57	0.9756	52.36	0.9981	44.29	0.9975
0.15	102.87	0.9808	99.26	0.9771	45.02	0.9983	35.41	0.9834
0.20	106.03	0.9841	104.02	0.9425	37.65	0.9947	28.21	0.9911
0.25	105.46	0.9879	101.85	0.9855	31.7	1.0000	22.4	0.9826
0.30	107.2	0.9877	103.63	0.9853	32.16	0.9976	21.91	0.9961
0.35	108.41	0.9882	104.86	0.9859	31.17	0.9976	20.69	0.9961
0.40	103.86	0.9835	100.03	0.9802	30.81	0.9972	20.19	0.9952
0.45	101.2	0.9912	97.19	0.9894	30.3	0.9581	20.61	0.9933
0.50	101.79	0.9900	97.76	0.9879	30.8	0.9939	20.77	0.9878
0.55	104.87	0.9895	100.96	0.9873	31.91	0.9929	21.13	0.9856
0.60	105.72	0.9909	101.82	0.9891	32.14	0.9900	21.31	0.9790
0.65	105.72	0.9935	104.78	0.9921	32.5	0.9859	21.64	0.9698
0.70	109.01	0.9899	105.21	0.9879	33.49	0.9825	22.61	0.9625
0.75	110.15	0.9986	106.38	0.9899	34.34	0.9816	23.43	0.9613
0.80	109.86	0.9891	106.05	0.9869	35.14	0.9809	24.21	0.9589
0.85	108.15	0.9835	104.22	0.9803	35.77	0.9749	24.8	0.9478
0.90	105.41	0.9814	101.3	0.9776	36.42	0.9742	25.42	0.9468
0.95	90.49	0.9523	85.53	0.9412	37.43	0.9770	26.39	0.9535

Kinetic analysis

The FWO and KAS model-free isoconversional methods were used for the calculation of the activation energies, E_a of decomposition reactions for the conversion degree, α varying in the range of 0.05–0.95 in a step of 0.05. The ICTAC kinetic committee has recommended to determine the E_a values in a wide range of between 0.05 and 0.95 with increments of 0.05 [33]. The main assumption of these methods is that the reaction mechanism does not change with reaction conversion (α), temperature and heating rate. The final equations of these methods as follows [34–42]:

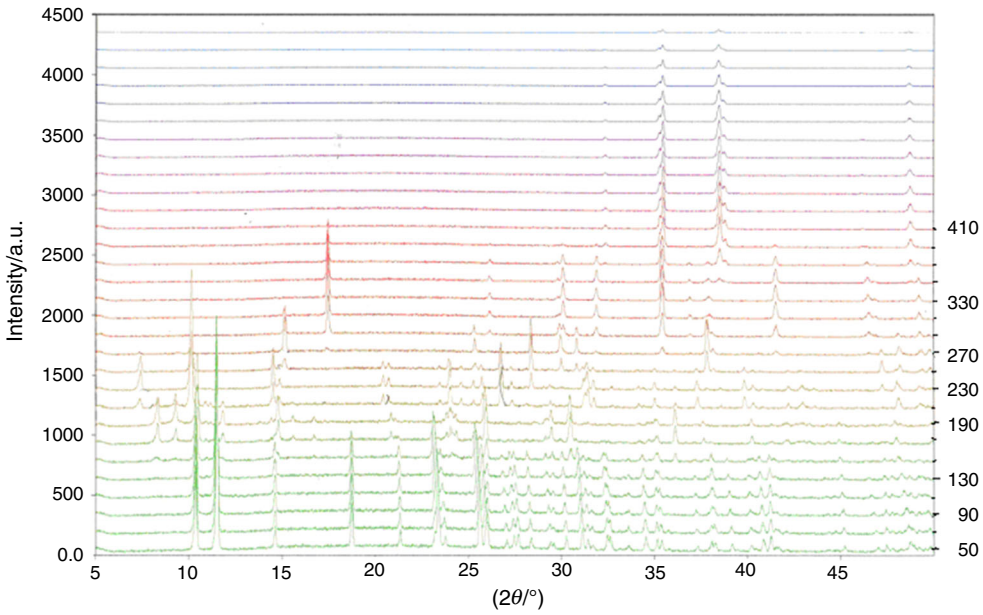

Fig. 6 High-temperature powder diffraction (HT-XRD) patterns of the $[CuPy_2Cl_2]$

FWO equation:

$$\ln \beta = \left[\frac{A \cdot E_a}{R \cdot g(\alpha)}\right] - 5.3305 - 1.05178\frac{E_a}{R}.\frac{1}{T} \quad (3)$$

and KAS equation:

$$\ln \frac{\beta}{T^2} = \left[\ln \frac{AR}{g(\alpha)E_a}\right] - \frac{E_a}{R}.\frac{1}{T} \quad (4)$$

where α is the degree of conversion, A is the pre-exponential factor, E_a is the activation energy, $g(\alpha)$ is an unknown function of the conversion, and R is the gas constant.

The graphs of $\ln\beta$ versus $1/T$ (for FWO equation) and the graphs of $\ln\beta/T^2$ versus $1/T$ (for KAS equation) are prepared for α constant. Apparent activation energies can be calculated with the use of slope values of these graphs. It was observed that the E_a values calculated using methods slightly differ from each other, whereas they show quite similar α-dependent behavior for all decomposition stages. The calculated values for the activation energies of all decomposition step of the $[CuPy_2Cl_2]$ with respect to decomposition ratio are shown in Fig. 5.

In the stage I, the activation energy values increase with an increase in decomposition ratio, α and reach to 87.65 kJ mol^{-1} at $\alpha = 0.35$. The E_a values remain relatively constant α values between 0.35 and 0.95. Therefore, it is concluded that the decomposition occurs multi-step except in the range of 0.35–0.95 where decomposition occurs only in one step (Fig. 5a). The average E_a values are 86.71 kJ mol^{-1} for FWO and 83.83 kJ mol^{-1} for KAS methods, respectively.

In the stage II, the activation energy, E_a, values persistently increase as α increase up to 0.45 and then decrease in the range of $0.45 \leq \alpha \leq 0.55$ and then start to increase up to 0.95 (Fig. 5b). Therefore, it is concluded that the decomposition takes place at least in two steps [43]. The average E_a values are 91.19 kJ mol^{-1} for FWO and 87.74 kJ mol^{-1} for KAS methods, respectively.

In the stage III, the E_a values decrease with increasing α up to $\alpha = 0.15$ and then increase up to $\alpha = 0.30$ and then decrease in the range of $0.30 \leq \alpha \leq 0.40$. The activation energy values increase again up to $\alpha = 0.75$ and then very fast decrease up to 0.95 (Fig. 5c). Therefore, it is concluded that the decompositions contain multi-step kinetics. The average E_a values are 105.15 kJ mol^{-1} for FWO and 101.76 kJ mol^{-1} for KAS methods, respectively.

In the stage IV, the E_a values decrease with increasing α up to $\alpha = 0.25$ and then remain relatively constant in α values between 0.25 and 0.95. Therefore, it is concluded that the decomposition occurs multi-step in the range of 0.05–0.25. The decomposition occurs only one step in the range of 0.25–0.95 (Fig. 5d). The average E_a values are 36.54 kJ mol^{-1} for FWO and 26.33 kJ mol^{-1} for KAS methods, respectively. The activation energy, E_a, values of all decomposition stages (kJ mol^{-1}) are tabulated in Table 3.

HT-XRD studies of the $[CuPy_2Cl_2]$

High-temperature powder diffraction (HT-XRD) patterns of the $[CuPy_2Cl_2]$ (PDF: 00-014-0991) measured for every 20 °C increase in temperature between 25 and 600 °C are

shown in Fig. 6. Accordingly, the complex is stable up to 130 °C, and the intermediate 2 begins to occur above 130 °C and transformation is completed at 235 °C. At this point, the intermediate 3 starts to occur, and also the transformation is completed at 270 °C. After this step, intermediate 3 is decomposed into intermediate 4 as given $CuCl_2$ formula (PDF: 00-001-0185) at 270 °C. Further, this product returns to CuO after 400 °C (PDF: 5-661) under air atmosphere. The results showed that the thermal decomposition intermediates (2 and 3) are new phases and there is any certain information of these phases in the literature. The XRD pattern of the complex indexed as $[CuPy_2Cl_2]$ (PDF: 00-014-991) has a monoclinic crystal system, P21/n (14) space group with $a = 16.9673$ Å, $b = 8.5596$ Å, $c = 3.8479$ Å; $\alpha = \gamma = 90.00°$, $\beta = 91.98°$, $V = 558.51$ Å^3 and $Z = 2.00$.

Conclusions

The $[CuPy_2Cl_2]$ was prepared by known synthesis method, and its intermediates (2 and 3 which are $[CuPyCl_2]$ and $[CuPy_{2/3}Cl_2]$) were prepared separately at 217 and 245 °C temperatures which were chosen from TG curve by using a tube furnace under N_2 atmosphere and characterized. Diffuse reflectance spectra of the $[CuPy_2Cl_2]$ and intermediates show a broad band is observed 700 nm (14,409 cm^{-1}) attributed to $^2A_{1g} \rightarrow {}^2B_{1g}$ and $^2B_{1g} \rightarrow {}^2E_g$ transitions which correspond to pseudo-tetrahedral coordination structure. In far-IR spectra of the $[CuPy_2Cl_2]$ and intermediates (2 and 3), Cu–Cl, Cu–N and C–H vibration bands are observed. However, far-IR spectrum of the intermediate 4 shows only Cu–Cl bands. These bands correspond to the bridge bonding. The spectroscopic results revealed that the coordination number of 4 was retained in the intermediates even if all the pyridine ligands were separated. The molecular ion peaks of 2 and 3 were observed as $[M+H]^+$ ($m/z = 214.978$), $[M-H]^+$ ($m/z = 185.614$) and $[M+C_2H_3O]^+$ ($m/z = 221.002$) from MALDI-TOF MS spectra. These results revealed the suggested structures for 2 and 3 are true. HT-XRD results show that $[CuPyCl_2]$ and $[CuPy_{2/3}Cl_2]$ intermediates are new phases formed at the end of the first and second decomposition steps. Thermal behaviors of the $[CuPy_2Cl_2]$ also investigated. The TG plot of the $[CuPy_2Cl_2]$ shows four decomposition steps. Average E_a values of these steps have been calculated as 85.27, 89.46, 103.46 and 31.41 kJ mol^{-1}, respectively.

Acknowledgements The authors would like to thank the Mersin University Research Fund for providing financial support to this study (Project Nr: BAP-FBE KB (TY) 2006-3 DR).

References

1. Bowman PB, Rogers LB. Effect of metal ion and ligand on thermal stability of metal amine complexes. J Inorg Nucl Chem. 1966;28:2215–24.
2. Ozawa T. A new method of analyzing thermogravimetric data. Bull Chem Soc Jpn. 1965;38:1881–6.
3. Mortimer CT, McNaughton JL. The thermal decomposition of transition—metal complexes containing heterocyclic ligands: 4. Substituted—pyridine complexes of Mn, Ni, Cu and Cd. Thermochim Acta. 1974;10:207–10.
4. Lıptay G, Burger K, Papp-Molnar E, Szebeni SZ, Ruff F. The thermal analysis of metal complexes—II: on the mixed pyridine-thiocyanate complexes of transition metals. J Inorg Nucl Chem. 1969;31:2359–66.
5. Wyrzykowski D, Styczen E, Warnke Z. Crystal structure of Co(3-pic)$_2$Cl$_2$ and thermal behaviour of a new complex, Co(py)(3-pic)Cl$_2$. Trans Met Chem. 2006;3:860–5.
6. Bond MR, Willett RD. An update of pseudoplanar, bridges $Cu_nX^{2-}_{n+2}$, $Cu_nX_{n+1}L^-$, $CunX_nL^2$ oligomer stacking patterns:structure of 1,2-dimethylpiridinumbis(μ-chloro)trichloroaquadicuprate(II). Inorg Chem. 1989;28:3228–67.
7. Nelson HC, Simonsen S H, Watt GW. Novel methadone salt containing a discrete, square-planar $CuCl_4^{2-}$ anion: X-ray crystal and molecular structure of bis(1-methyl-4-oxo-3,3-diphenylhexyldimethylammonium) tetrachlorocuprate(II). J Chem Soc Chem Commun. 1979;14:632–3.
8. Bukowska-Strzyzewska M, Skoweranda J. Structure of thermochromic crystals of benzimidazolium tetrachlorocuprate(II) hydrate. Acta Cryst. 1987;C43:2290–3.
9. Bukowska-Strzyzewska M, Wnek J, Tosik A, Glowiak T. Structure of polymeric bis(benzimidazolium) hexachlorodicuprate(II), $2C_7H_7N_2^+.Cu_2Cl_6^{2-}$. Acta Crystallogr. 1985;C41:1184–6.
10. Haddad S, Willett RD. Polymorphism in bis(4-dimethylaminopyridinium)tetrachlorocuprate(II). Inorg Chem. 2001;40:2457–60.
11. Bhattacharya R, Ghosh A, Ray MS, Righi L, Bocelli G, Chaudhuri S, Willett RD, Clemente-Juan, JM, Coronado E, Gomez-Garcia CJ. Synthesis, crystal structure, thermal analysis and magnetic behavior of a novel one-dimensional polymeric pyridinium chlorocuprate(II): $(Hpy)_2[Cu_3Cl_8(H_2O)_2]$. Eur J Inorg Chem. 2003;23:4253–9.
12. Grant D, Payne DS. Pyrophosphite as a ligand. J Inorg Nucl Chem. 1964;26:1985–90.
13. Allan JR, Brown DH, Nuttall RH, Sharp DWA. The thermal decomposition of metal complexes—IV: the preparation and thermal decomposition of some pyridine and substituted-pyridine complexes of nickel (II) halides. J Inorg Nucl Chem. 1965;27:1529–36.
14. Bowman PB, Rogers LB. Effect of metal ion and ligand on thermal stability of metal amine complexes. J Inorg Nucl Chem. 1966;28:2215–24.
15. Mortimer CT, McNaughton JL. The thermal decomposition of transition metal containing heterocyclic ligands-Substituted pyridine complexes of cobalt. Thermochim Acta. 1974;10:125–8.
16. Mortimer CT, McNaughton JL. The thermal decomposition of transition metal containing heterocyclic ligands-Substituted pyridine complexes of Mn, Ni, Cu, and Cd. Thermochim Acta. 1974;10:207–10.
17. Allan JR, Carson BR. Thermal, spectral and magnetic studies of some first row transition metal complexes of 2-(p-tolyl)pyridine. Thermochim Acta. 1990;160:329–35.
18. Farran R, House JE. Thermal decomposition of complexes of palladium(II) chloride with substituted pyridines. J Inorg Nucl Chem. 1972;34:2219–23.

19. Goher MAS. Thermal analysis of some cobalt(II) azido complexes of the type $CoL_4(N_3)_2$ for L = pyridine derivative ligands. Thermochim Acta. 1999;336:61–4.
20. Szecsenyi KM, Wadsten T, Carson B, Bencze E, Kenessey G, Liptay G. Pyridine type complexes of transition metal halides, XIII. Solid-state studies of copper(II)-chloride and bromide complexes with methylpyridines. Part II: complexes with 2- and 4-methylpyridine and 2,4,6-collidine. Thermochim Acta. 1999;340–341:255–61.
21. Perez J, Sanchez G, Garcia J, Serrano JL, Lopez G. Thermal and kinetic analysis of ortho-palladated complexes with pyridines. Thermochim Acta. 2000;362:59–70.
22. Xu GC, Zhang L, Liu GF, Jia DZ. Thermal kinetic TG-analysis of the mixed ligand copper(II) and nickel(II) complexes of *N*-(1-phenyl-3-methyl-4-benzylidine-5-pyrazolone) p-nitrobenzoylhydrazide and pyridine. Thermochim Acta. 2005;429:31–42.
23. Cılgı GK, Cetisli H, Donat R. Thermal and kinetic analysis of uranium salts. J Therm Anal Calorim. 2012;110:127–35.
24. Ocakoglu K, Emen FM. Thermal analysis of cis-(dithiocyanato)(1,10-phenanthroline-5,6-dione)(4,40-dicarboxy-2,20-bipyridyl)ruthenium (II) photosensitizer. J Therm Anal Calorim. 2011;104:1017–22.
25. Kaljuvee T, Rudjak I, Edro E, Trikkel A. Heating rate effect on the thermal behavior of ammonium nitrate and its blends with limestone and dolomite. J Therm Anal Calorim. 2009;97:215–21.
26. Kang SK, Kim HS, Kim YI. Synthesis and characterisation of pseudotetrahedral copper(II) dihalide complexes with (s)-(-)-nicotine. Bull Korean Chem Soc. 2004;25:1959–62.
27. Costamagna J, Caruso F, Vargas J, Manriquez V. Planar or tetrahedral coordination in copper(II) complexes induced by bromo substitution. Inorg Chim Acta. 1998;267:151–8.
28. Emandi A, Nicolae A, Badea M, and Olar R. Synthesis and characterisation of some new complexes of Ni(II), Cu(II), Zn(II), Cd(II) and Hg(II) with mixed ligands (nitrogen, oxygen) donor groups. Chimie, Anul XIII Analele University Bucureşti, 2004;I–II:167–172.
29. Nair MS, Joseyphus RS. Synthesis and characterisation of Co(II), Ni(II), Cu(II) and Zn(II) complexes of tridentate Schiff base derived from vanillin and DL-α-aminobutyric acid. Spectrochim Acta A. 2007;70:749–53.
30. Sathyanarayana DN. Electronic absorption spectroscopy and related techniques. Kindle ed. Chemistry: Universities Press (India) Limited; 2001.
31. Wong PT, Brewer DG. Nature of the coordination bond in metal complexes of substituted pyridine derivatives—II: the far infrared spectra and metal-ligand force constant of copper complexes of 4-substituted pyridines. Can J Chem. 1968;46:139–48.
32. Clark RJH, Williams CS. The far infrared spectra of metal-halide complexes of pyridine and related ligands. Inorg Chem. 1964;4:350–7.
33. Vyazovkin S, Burnham AK, Criado JM, Maqueda LAP, Popescu C, Sbirrazzuoli N. ICTAC Kinetics Committee recommendations for performing kinetic computations on thermal analysis data. Thermochim Acta. 2011;520:1–19.
34. Chaiyo N, Muanghlua R, Niemcharoen S, Boonchom B, Seeharaj P, Vittayakorn N. Non- isothermal kinetics of the thermal decomposition of sodium oxalate Na_2C_2O4. J Therm Anal Calorim. 2012;107:1023–9.
35. Vecchio S, Materazzi S, Kurdziel K. Thermal decomposition kinetics of palladium(II)1-allylimidazole complexes. Int J Chem Kinet. 2005;37:667–74.
36. Koyundereli Cilgi G, Cetişli H. Thermal decomposition kinetics of aluminum sulfate hydrate. J Therm Anal Calorim. 2009;98:855–61.
37. Emen FM, Ocakoglu K, Kulcu N. An investigation of decomposition stages of a ruthenium polypridyl complex by non-isothermal methods. J Therm Anal Calorim. 2012;110:799–805.
38. Soyleyici S, Koyundereli Cilgi G. Thermal and kinetic analyses of 2,5-bis(2-hydroxyphenyl) thiazolo[5,4-d]thiazole. J Therm Anal Calorim. 2014;118:705–9.
39. Alves APM, Araujo AS, Bezerra FA, Sousa KS, Lima SJG, Fonseca MG. Kinetics of dehydration and textural characterizations of selectively leached vermiculites. J Therm Anal Calorim. 2014;117:19–26.
40. Fandaruff C, Araya-Sibaja AM, Pereira RN, Hoffmeister CRD, Rocha HVA, Silva MAS. Thermal behavior and decomposition kinetics of efavirenz under isothermal and non-isothermal conditions. J Therm Anal Calorim. 2014;115:2351–6.
41. Hu C, Mi J, Shang S, Shangguan J. The study of thermal decomposition kinetics of zinc oxide formation from zinc oxalate dihydrate. J Therm Anal Calorim. 2014;115:1119–25.
42. Arora S, Aneja DK, Kumar M, Sharma C, Prakas O. Thermal studies of some biological active oxadiazoles non-isothermal kinetic study of potent antibacterial 2-(4-chlorophenyl)-5-(thiophen-2-yl)-1,3,4-oxadiazole. J Therm Anal Calorim. 2013;111:17–25.
43. Fajnor VS, Jesenák K. Differential thermal analysis of montmorillonite. J Therm Anal Calorim. 1996;46(2):489–93.